Nuclear Instruments and Methods in Physics Research A 634 (2011) 52–58

Contents lists available at ScienceDirect

Nuclear Instruments and Methods in Physics Research A

journal homepage: www.elsevier.com/locate/nima

Focusing X-ray spectrograph with spatial resolution and uniform dispersion

Qingguo Yang *, Yan Ye, Guanghua Chen, Zeren Li, Libing Yang, Qixian Peng, Xianbin Huang, Hongchun Cai, Jing Li

Institute of Fluid Physics, CAEP, P.O. Box 919-109, Mianyang, Sichuan 621900, PR China

ARTICLE INFO

Article history:
Received 16 September 2010
Received in revised form
9 January 2011
Accepted 11 January 2011
Available online 21 January 2011

Keywords:
X-ray spectrograph
Focusing
Spatial resolution
Uniform dispersion

ABSTRACT

A new focusing X-ray spectrograph with spatial resolution and uniform dispersion (FSSRUD) is proposed. Uniform dispersion (i.e., the linear dispersion is a constance, or in other words, the X-rays are dispersed on the detector with uniform spacing for every wavelength) can be realized by bending the crystal of a spectrograph into a special shape. Since the spatial coordinate of the spectrum obtained by the FSSRUD varies linearly with X-ray wavelength, it is very convenient for identification and processing of the experimental data. In addition, an optimized spectrograph capability can be achieved by customizing the bent shape of the crystal and other spectrograph parameters to satisfy the given requirements of routine measurement. The spectrograph capability is first analyzed using a ray tracing method, the principle to design the shape of the crystal for the FSSRUD is then presented and the numerical evaluations are used to validate its effectiveness.

1. Introduction

X-ray imaging spectroscopy is a powerful tool for investigating hot, dense plasmas [1,2]. The development of appropriate X-ray crystal spectrograph is of great interest to the Z pinch and laser plasma physics communities. The focusing X-ray spectrograph with spatial resolution, due to its high luminosity, high spectral and spatial resolution, has been the main goals of new spectrograph development. The simplest scheme of focusing X-ray spectrograph is the cylindrically von Hamos scheme [3], which is widely used in laser plasma [4,5] and electron beam ion trap (EBIT) experiments [6]. In this scheme, the linear dispersion and aberrations increase rapidly with decrease of Bragg angle, so that the crystal must be placed close to the source if the Bragg angle is not very small and if a reasonable spectral band is wanted. In order to reduce the dispersion length to match with the electronic detector (e.g., the streak camera or the X-ray CCD) and to enlarge the distance between source and crystal to alleviate the damage of crystal from the plasma debris, an extreme luminosity imaging conical spectrograph (ELICS) [7] is suggested. In this configuration, the source and the detector are all positioned on the cone axis, the cone surface acts as a focusing cylindrical mirror and forms an image on the film or detector. In the case of line radiation, the spectrograph will give two-dimensional images in each spectral line. The drawbacks of this spectrograph are narrower spectral band, lower spectral resolution and higher aberrations compared to the focusing X-ray spectrograph with spatials resolution (FSSR) based on spherically bent crystal. Owing to its universality (i.e., crystal with any radius of curvature can be used in any experiment and tuned to the spectral lines in a wide spectral band), high luminosity, high spectral and spatial resolution, the FSSR has now been the most widely used spectrograph in the plasma diagnoses [8–19].

However, it should be noticed that all the spectrographs mentioned above have a common character: the linear dispersion of these spectrographs is varying with X-ray wavelength across the spectral band, or in other words, the X-rays are non-uniformly dispersed on the detector. Non-uniform dispersion has the following drawbacks: (1) The spectrum recorded by the detector needs a coordinate correction according to the geometrical configuration of spectrograph to restore an actual distribution of spectral intensity as a function of wavelength. The processing of spectrum is inconvenient since the code to restore the spectrum must be modified every time if any parameters of the spectrograph is changed; (2) Non-uniform dispersion may cause resolving problems due to limited resolving power of detector. For example, if the linear dispersion of a spectrograph varies from a very small value to a very large value, the smallest linear dispersion may result in failure of resolving two neighboring lines, while the largest linear dispersion will waste the valuable detecting area. Therefore, in practice the applicable spectral band used is usually a band in which the linear dispersion varies slowly.

In fact, the linear dispersion of a focusing X-ray spectrograph is determined by the bent curve of the crystal in the dispersion direction (spectral direction), so an uniform dispersion spectrograph can be realized if the shape of the bent crystal is properly designed. The focusing X-ray spectrograph with spatial resolution and uniform dispersion (FSSRUD) would benefit from the following advantages: (1) No coordinate correction to be required. (2) It is convenient for spectrum identification. For example, one can

* Corresponding author.
E-mail address: yungore@163.com (Q. Yang).

0168-9002/$ - see front matter
doi:10.1016/j.nima.2011.01.032

easily identify an unknown spectral line by the inquiry of the database of ion spectrum according to the distance between the well known and the unknown. (3) An optimized spectrograph capability can be achieved by customizing the spectrograph parameters to satisfy the given requirements of experiment. That is, if the spectral band, the dispersion length (determined by the dimension of detector), the distance of source to crystal, the solid angle of crystal expanded to source and other experimental conditions are preassigned, the bent shape of the crystal, the linear dispersion, the spectral resolution, the luminosity and other parameters can be optimized to satisfy the given requirements. These issues motivate the current work.

2. Focusing X-ray spectrograph with spatial resolution

2.1. General characteristics

For a focusing spectrograph, the diffraction plane of the crystal is usually bent into a cylindrically symmetric form. If a point source is located on the symmetry axis of the bent crystal, as shown in Fig. 1, all X-rays with the same wavelength leaving the point source, upon reflection from the crystal with the same grazing angle, will be focused on the symmetry axis again and produce point-to-point imaging in monochromatic radiation in the sagittal plane (the plane perpendicular to symmetry axis). Meanwhile, the X-rays with different wavelengths will be dispersed along the crystal surface in the meridional plane (the plane containing the symmetry axis and the center of the crystal) according to the Bragg condition:

$$2d\sin\theta = n\lambda \tag{1}$$

where θ is the grazing angle, λ is the radiation wavelength, n is the diffraction order and d is the crystal constance.

2.2. Mathematical description of spectrograph capability

For analysis of spectrograph capability, one way is to build a mathematical model based on ray tracing. Since the profile of the crystal for a focusing X-ray spectrograph is cylindrical symmetry, the shape of the crystal can be described by the curve intersected by the meridional plane and crystal surface (i.e., the profile curve or the bent curve for a cylindrical symmetry surface). If a coordinate system is built as shown in Fig. 2, in which the source location is selected as the origin and the symmetry axis as the X axis, the bent curve of the crystal can be presented as

$$r = r(\varphi) \tag{2}$$

where φ is the polar angle between an incident radiation and the X axis. The unit vector of tangent line for this curve at point (r,φ) and the unit vector of incident ray are written, respectively, as

$$\mathbf{T} = (r^2+r'^2)^{1/2}(r'\cos\varphi - r\sin\varphi, r'\sin\varphi + r\cos\varphi) \tag{3}$$

$$\mathbf{I} = (\cos\varphi, \sin\varphi) \tag{4}$$

where $r' = \mathrm{d}r/\mathrm{d}\varphi$. From a geometric point of view, the diffraction of X-rays from the surface of a crystal can be considered as the

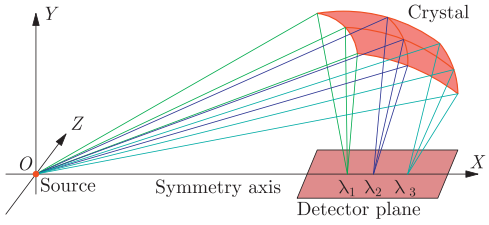

Fig. 1. Diagram showing the concept of the focusing X-ray spectrograph.

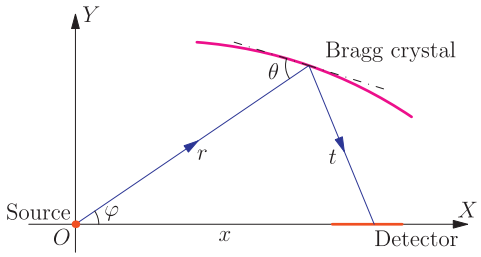

Fig. 2. Coordinate system built for the focusing X-ray spectrograph in the meridional plane.

mirror reflection, so that the unit vector of reflected ray can be calculated by the reflection law as

$$\mathbf{R} = 2(\mathbf{I}\cdot\mathbf{T})\mathbf{T} - \mathbf{I}. \tag{5}$$

By using this unit vector, the spatial coordinate x for the intersection point of the reflected ray with the X axis (where a detecting plane is positioned) is determined by

$$x = \frac{2r^2r'}{(r'^2-r^2)\sin\varphi + 2rr'\cos\varphi}. \tag{6}$$

Considering the fact that $\sin\theta = |\mathbf{I}\times\mathbf{T}|$, the X-ray wavelength λ is then presented as

$$\lambda = \frac{2d}{n}\frac{r}{\sqrt{r^2+r'^2}}. \tag{7}$$

Eqs. (6) and (7) build the bridge over the key parameters x and λ through the bent curve $r(\varphi)$ and its derivative. The rest parameters of spectrograph can be deduced from these two parameters.

The linear dispersion defined by $\mathrm{d}x/\mathrm{d}\lambda$ is

$$\frac{\mathrm{d}x}{\mathrm{d}\lambda} = \frac{\mathrm{d}x}{\mathrm{d}\varphi}\left(\frac{\mathrm{d}\lambda}{\mathrm{d}\varphi}\right)^{-1} = \frac{nr(r^2+r'^2)^{5/2}[2r'^2\sin\varphi + r(r'\cos\varphi - r''\sin\varphi)]}{dr'(r'^2-rr'')[(r'^2-r^2)\sin\varphi + 2rr'\cos\varphi]^2} \tag{8}$$

where $r'' = \mathrm{d}^2r/\mathrm{d}\varphi^2$.

The magnification in the sagittal plane (spatial direction) is simply given by

$$M_{\mathbf{spat}} = t/r = \frac{(r^2+r'^2)\sin\varphi}{(r^2-r'^2)\sin\varphi - 2rr'\cos\varphi} \tag{9}$$

where $t = (r^2+x^2-2rx\cos\varphi)^{1/2}$, is the path length of reflected ray which satisfies the following imaging equation:

$$1/r + 1/t = 1/f \tag{10}$$

where f is the focal length of crystal in the spatial direction. The calculation of the magnification in the meridional plane (spectral direction) is more complicated. As is well known, if the radiation is not monochromatic, but consists of separate narrow spectral lines (i.e., $\Delta\lambda/\lambda$ is not large), or the source size D is not very small (i.e., $D \gg M_{\mathrm{spectr}}^{-1}\Delta\lambda\mathrm{d}x/\mathrm{d}\lambda$, where M_{spectr} is the magnification in the meridional plane given below), spatial imaging in the meridional plane is possible. These conditions can be easily satisfied in the multi-wire arrays Z pinch experiments, where radiation sources are in a centimeter size scale. (e.g., $M_{\mathrm{spectr}}^{-1}\Delta\lambda\mathrm{d}x/\mathrm{d}\lambda$ is about 0.4 mm for a spherical mica crystal spectrograph if the wavelength is 1.5 nm, source size is 2 mm, spherical radius is 200 mm and distance of source to spherical center is 600 mm.) Considering this fact, the magnification in the meridional plane is given by (See Appendix A)

$$M_{\mathbf{spectr}} = \frac{(r^2+r'^2)^2[3r'^2\sin\varphi + r(2r'\cos\varphi - r''\sin\varphi)]}{(rr''-r'^2)[(r'^2-r^2)\sin\varphi + 2rr'\cos\varphi]^2}. \tag{11}$$

Because of the imaging properties of the spectrograph in the spectral direction, the actual spectral resolution is dependent on the

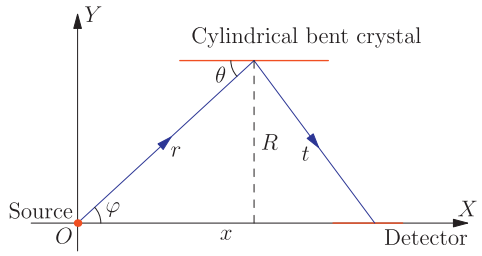

Fig. 3. Geometry of the cylindrical von Homas spectrograph.

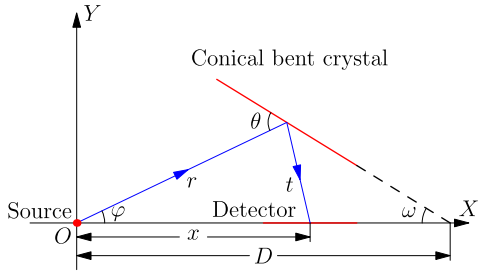

Fig. 4. Geometry of the conical ELICS spectrograph.

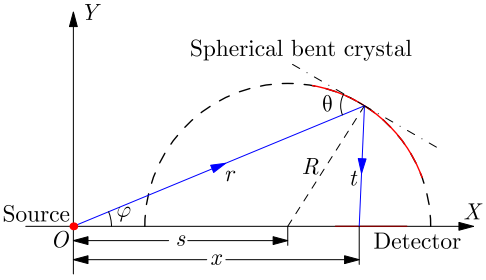

Fig. 5. Geometry of the spherical FSSR-2D spectrograph.

Table 1
Formulas of the major parameters for three typical focusing X-ray spectrographs with cylindrical von Hamos scheme, conical ELICS scheme and spherical FSSR-2D scheme.

	Cylindrical (von Hamos)	Conical (ELICS)	Spherical (FSSR-2D)
$r(\varphi)$	$R\csc\varphi$	$\frac{D}{\cos\varphi+\cot\omega\sin\varphi}$	$s\cos\varphi+\chi$
x	$2R\cot\varphi$	$D-\frac{D\sin\varphi}{\sin(\varphi+2\omega)}$	$\frac{2s\chi(\chi+s\cos\varphi)}{\kappa}$
λ	$\frac{2d\sin\varphi}{n}$	$\frac{2d\sin(\varphi+\omega)}{n}$	$\frac{2d\chi}{nR}$
$\frac{dx}{d\lambda}$	$\frac{-nR}{d\cos\varphi\sin^2\varphi}$	$\frac{-nD\sin2\omega}{2d\sin^2(\varphi+2\omega)\cos(\varphi+\omega)}$	$\frac{-nR^3(\chi+s\cos\varphi)^2}{d\kappa^2\cos\varphi}$
M_{spat}	1	$\frac{\sin\varphi}{\sin(\varphi+2\omega)}$	$\frac{R^2}{\kappa}$
M_{spectr}	$-\csc\varphi$	$-\csc(\varphi+2\omega)$	$\frac{2R^2\eta}{\kappa^2(\chi+s\cos\varphi)\sin2\varphi}$
$\frac{\Delta\lambda}{\lambda}$	$\frac{\Delta S\sin2\varphi}{4R}$	$\frac{\Delta S\sin\varphi\sin(\varphi+2\omega)}{D\tan(\varphi+\omega)\sin2\omega}$	$\frac{-\eta\Delta S}{2\chi(\chi+s\cos\varphi)^3}$
L_{total}	$\frac{w\sin^3\varphi}{R^2}$	$\frac{w\sin^2(\varphi+\omega)\sin^2(\varphi+2\omega)}{D^2\sin\varphi\sin^2\omega}$	$\frac{w\chi^2\kappa^2}{R^4s^2\sin\varphi(\chi+s\cos\varphi)^2}$

$\chi=(R^2-s^2\sin^2\varphi)^{1/2}$
$\kappa=2\chi^2+2s\chi\cos\varphi-R^2$
$\eta=[\chi^3-s(R^2-2\chi^2)\cos\varphi]\cos\varphi-s\chi(2\chi+3s\cos\varphi)\sin\varphi^2$

size of the source and it is useful to determine spectral bands, where the spatial contribution to the line shape will dominate the actual spectral line broadening. The shift of a line in spectral units $\Delta\lambda$ corresponding to a spatial shift Δs in the source plane is given by

$$\Delta\lambda=(d\lambda/dx)\Delta x=(d\lambda/dx)M_{spectr}\Delta s\sin\varphi. \quad (12)$$

Therefore, the effective spectral resolution is given by

$$\Delta\lambda/\lambda=\frac{r'\sin\varphi[r(r''\sin\varphi-2r'\cos\varphi)-3r'^2\sin\varphi]\Delta S}{2r^2[(2r'^2-rr'')\sin\varphi+rr'\cos\varphi]} \quad (13)$$

where ΔS is the average source size.

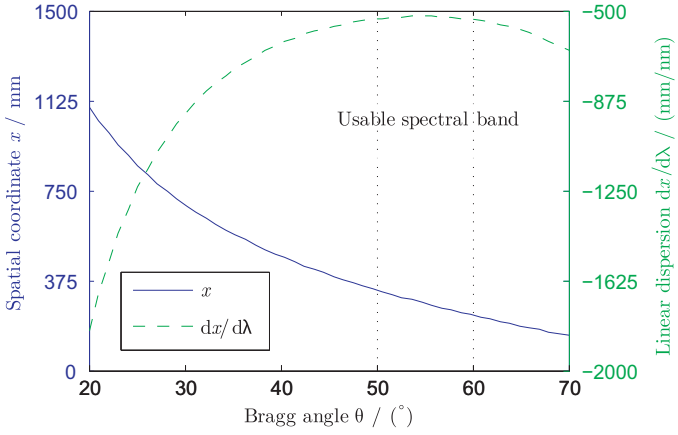

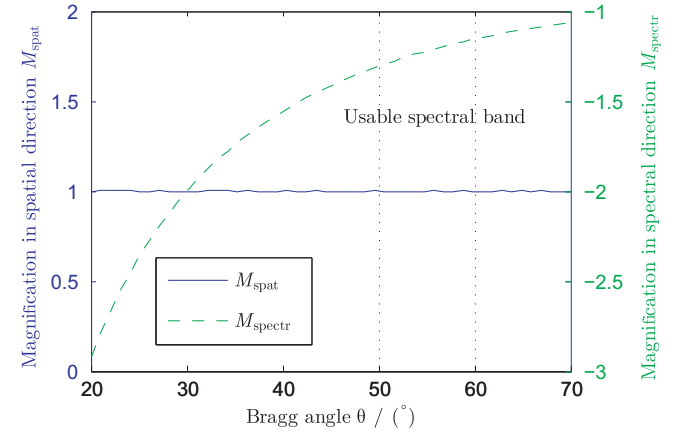

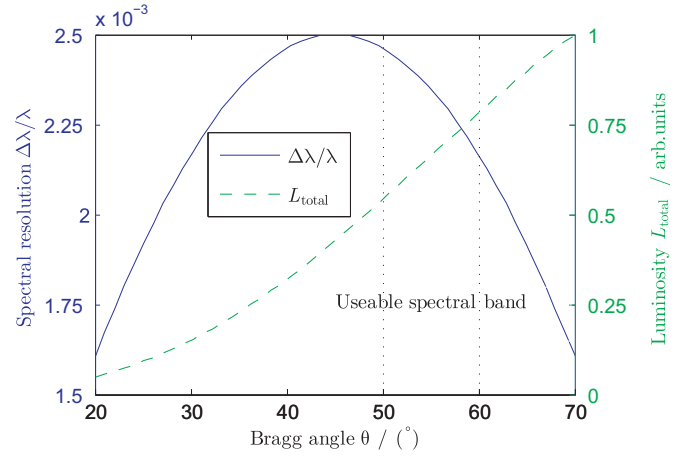

Fig. 6. The major parameters (x, $dx/d\lambda$, M_{spat}, M_{spectr}, $\Delta\lambda/\lambda$, L_{total}) of the focusing X-ray spectrograph with cylindrical von Hamos scheme as a function of Bragg grazing angle θ. The cylindrical radius R is 200 mm, crystal $2d$ spacing is 1.984 nm and the source size ΔS is 2 mm.

The luminosity of the spectrograph can be estimated if we take into account the acceptance angle in the spatial direction and the luminosity coefficient in the spectral direction [19]. In the spatial direction, the common parameter is $L_{spat}=w/f$, where w is the linear aperture of an optical system and f is the focal length given by Eq. (10). In the spectral direction, the luminosity coefficient can be estimate by $L_{spectr}=|d\varphi/dx|$. Therefore, the total luminosity of a focusing spectrograph is given by

$$L_{total}=L_{spat}L_{spectr}=\left|\frac{w(r-r'\cot\varphi)[(r'^2-r^2)\sin\varphi+2rr'\cos\varphi]^2}{r(r^2+r'^2)^2[(2r'^2-rr'')\sin\varphi+rr'\cos\varphi]}\right|. \quad (14)$$

The luminosity describes the ability of photons collection as a function of radiation wavelength for a focusing spectrograph and the normalized value is used to modify the intensity of recorded spectrum to eliminate the discrepancy brought by the spectrograph.

2.3. Investigation of three typical focusing X-ray spectrographs

In this subsection, three typical focusing X-ray spectrographs, the cylindrical von Hamos scheme, the conical ELICS scheme and the spherical FSSR-2D scheme (where the source and the detector plane are all placed along the symmetry axis of the spherically bent crystal) are investigated in detail. The geometry of these spectrographs are shown in Figs. 3–5, respectively. The corresponding formulas for

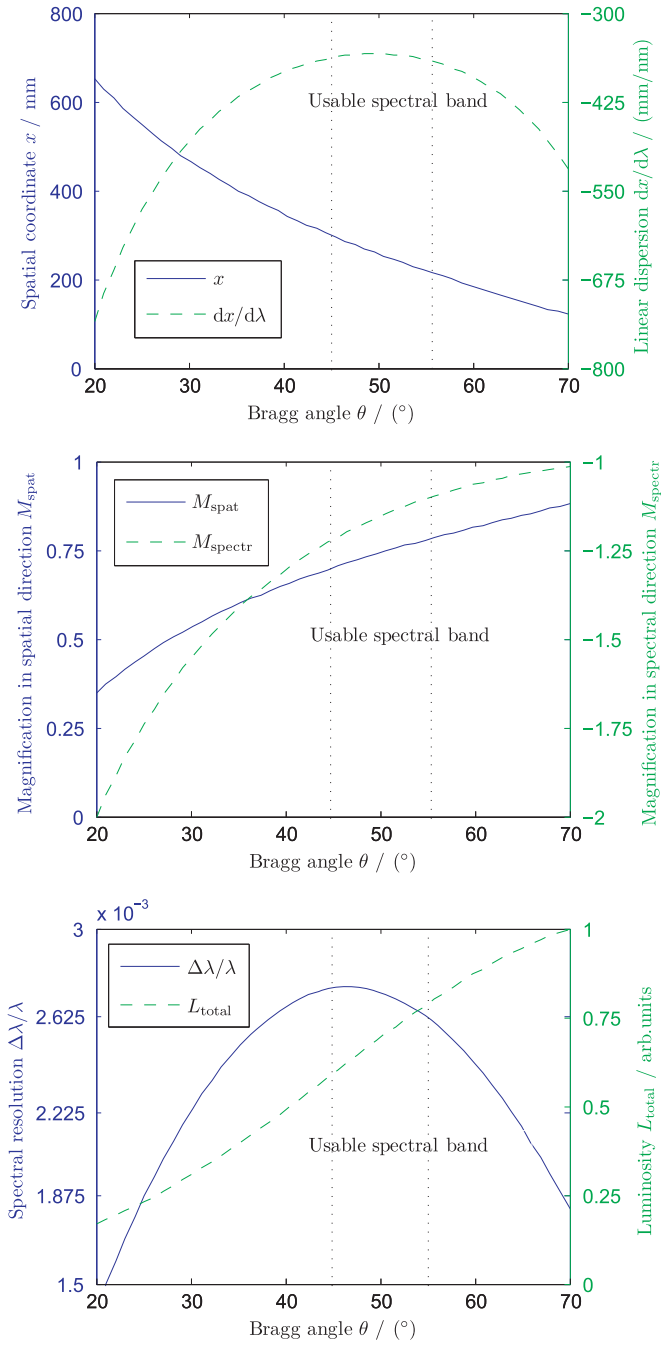

Fig. 7. The major parameters (x, $dx/d\lambda$, M_{spat}, M_{spectr}, $\Delta\lambda/\lambda$, L_{total}) of the focusing X-ray spectrograph with conical ELICS scheme as a function of Bragg grazing angle θ. The cone angle ω is 10°, distance of source to cone apex D is 1000 mm, crystal $2d$ spacing is 1.984 nm and the source size ΔS is 2 mm.

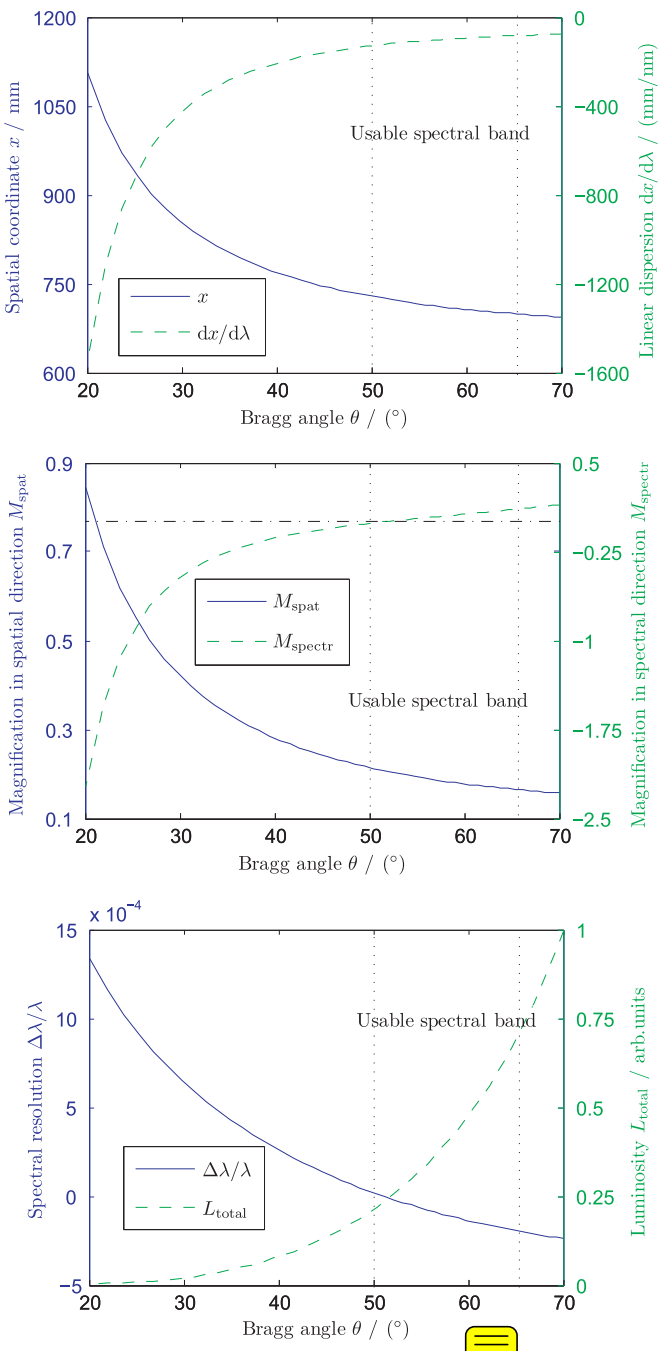

Fig. 8. The major parameters (x, $dx/d\lambda$, M_{spat}, M_{spectr}, $\Delta\lambda/\lambda$, L_{total}) of the focusing X-ray spectrograph with spherical FSSR-2D scheme as a function of Bragg grazing angle θ. The spherical radius R is 200 mm, distance of source to spherical center s is 600 mm, crystal $2d$ spacing is 1.984 nm and the source size ΔS is 2 mm.

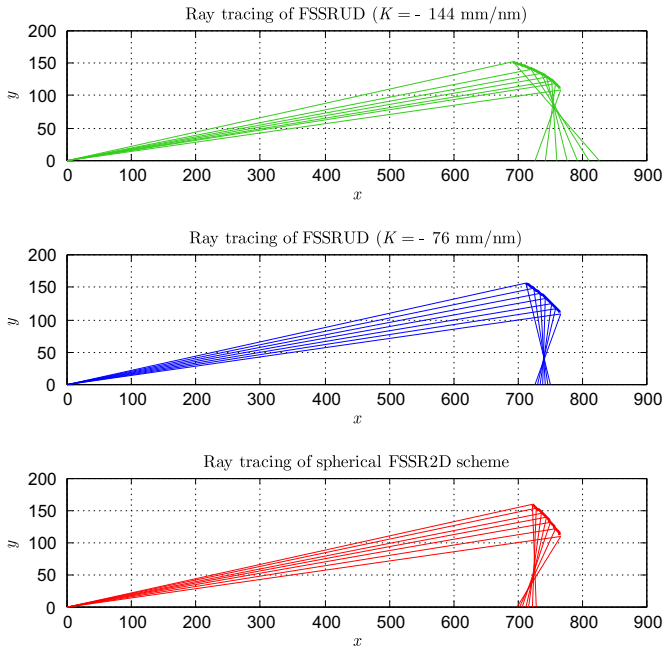

Fig. 9. Ray tracing diagrams for the spherical FSSR-2D spectrograph and two FSSRUDs.

describing the spectrograph capabilities are listed in Table 1. These formulas can be used to analyze the spectrograph analytically or numerically. The graphs of the major parameters (x, $\mathrm{d}x/\mathrm{d}\lambda$, M_{spat}, M_{spectr}, $\Delta\lambda/\lambda$, $Ł_{\mathrm{total}}$) vs the Bragg angle θ are, respectively, shown in Figs. 6–8. In these figures, θ ranges from 20° to 70° but only a small part of it (a narrow spectral band) are usable in practice due to limited crystal length and/or limited detecting area. (If a film is used as the detector, the FSSR-2D scheme can work as a wide-band spectrograph by combining three or more cuts of spatially shifted crystals as done in Ref. [19].) For the cylindrical von Hamos scheme as shown in Fig. 6, the linear dispersion decreases rapidly as θ decreases toward 20° and increases toward 70°, the usable spectral band is thus in the range [50°,60°], where the linear dispersion changes slowly as Bragg angle varies. The average absolute value of the linear dispersion in this range is about 528 mm/nm and the dispersion length is about 105 mm. The conical ELICS scheme (see Fig. 7) is similar to the cylindrical von Hamos scheme but with smaller average absolute value of linear dispersion (about 360 mm/nm) and dispersion length (about 80 mm) in the usable spectral band [45°,55°]. For the spherical FSSR-2D scheme as shown in Fig. 8, the absolute linear dispersion increases rapidly with the decrease of Bragg angle and the best spectral band is about the range [50°,65°]. The average absolute value of the linear dispersion is 102 mm/nm and the dispersion length is 29 mm, nearly matching with the dimension of the electronic detector.

3. Focusing X-ray spectrograph with spatial resolution and uniform dispersion

From Eq. (8), it can be seen that the linear dispersion of a focusing X-ray spectrographs is totally determined by the shape of the bent crystal in the meridional plane. If the shape of the bent crystal is properly designed, the realization of uniform dispersion is possible. Since the linear dispersion of a FSSRUD is a constance, the bent curve, $r(\varphi)$, of a FSSRUD must be satisfied with the following differential equation:

$$\frac{nr(r^2+r'^2)^{5/2}[2r'^2\sin\varphi+r(r'\cos\varphi-r''\sin\varphi)]}{dr'(r'^2-rr'')[(r'^2-r^2)\sin\varphi+2rr'\cos\varphi]^2}=K \qquad (15)$$

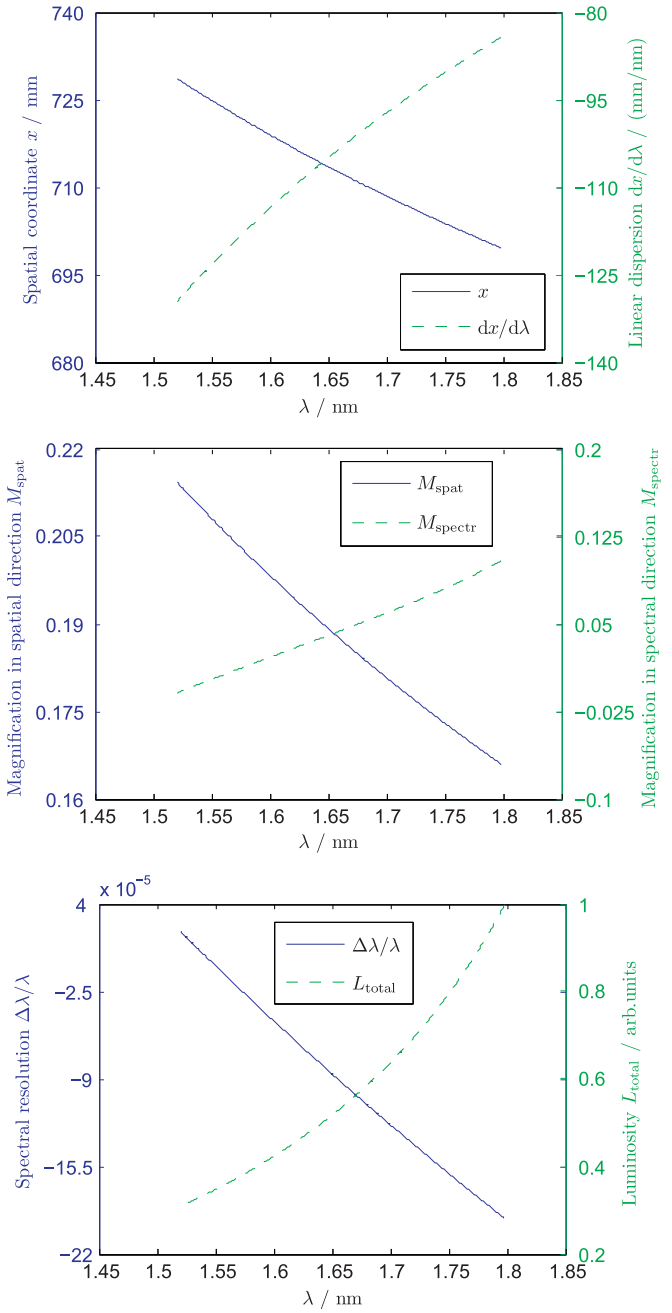

Fig. 10. The major parameters (x, $\mathrm{d}x/\mathrm{d}\lambda$, M_{spat}, M_{spectr}, $\Delta\lambda/\lambda$, $Ł_{\mathrm{total}}$) of a spherical FSSR-2D spectrograph as a function of wavelength λ. The spherical radius R is 200 mm, distance of source to spherical center s is 600 mm, crystal 2d spacing is 1.984 nm and the source size ΔS is 2 mm.

where K is the constant linear dispersion. The value of K can be positive or negative, but a negative value is preferred if a wide spectral band is desired. Eq. (15) has no analytical solutions but can be solved by a numerical method. If the initial conditions $r(\varphi_0)=r_0$ and $r'(\varphi_0)=r_0'$ ($r_0'<0$ should be satisfied) are given, the bent curve, $r(\varphi)$, of the crystal can be numerically computed in arbitrary accuracy, and then the data can be transferred to a digital controlled machine to fabricate the metal frame for bending the crystal.

To demonstrate the feasibility of the method proposed above, we give two designing examples and compare it with the spherical FSSR-2D scheme shown in Section 2.3. For comparative purpose, the crystal length (about 67.3 mm), the distance of source to one end of crystal (about 775 mm) and the angle of crystal expanded for radiative source (ranging from 8.1° to 12.4°) of two FSSRUDs are

required to be the same as the spherical FSSR-2D scheme are, so the initial conditions of two FSSRUDs are set as $r_0=775$ mm and $r_0'=-462$ mm. The linear dispersion of the first FSSRUD is -76 mm/nm and the second one is -144 mm/nm. Fig. 9 shows the ray tracing diagrams for the spherical FSSR-2D scheme and two FSSRUDs designed above. The sampled rays are uniformly distributed over the spectral band. It can be clearly seen that the rays of two FFSRUDs strick the detector with uniform spacing while the spherical FSSR-2D scheme is not. The FSSRUD with $K=-76$ mm/nm has a very small dispersion length (about 24 mm), which matches with the X-ray CCD detecting system better than the spherical FFSR2D scheme. In addition, in this configuration the X-ray is well focused and a small aperture near the quasi-focal point can be positioned to shield the background radiations. The FSSRUD with $K=-144$ mm/nm is designed for a film detecting system which has a large dispersion length (about 100 mm) and a wide spectral band. The plot of performance parameters (x, $\mathrm{d}x/\mathrm{d}\lambda$, M_{spat}, M_{spectr}, $\Delta\lambda/\lambda$, $Ł_{\mathrm{total}}$) vs wavelength λ of the spherical FSSR-2D scheme and two FSSRUDs are shown in Figs. 10–12, respectively. It can be seen that the capability of the FSSRUD with $K=-76$ mm/nm is similar to the spherical FSSR-2D scheme but with better performance in energy distribution. The former has a uniform

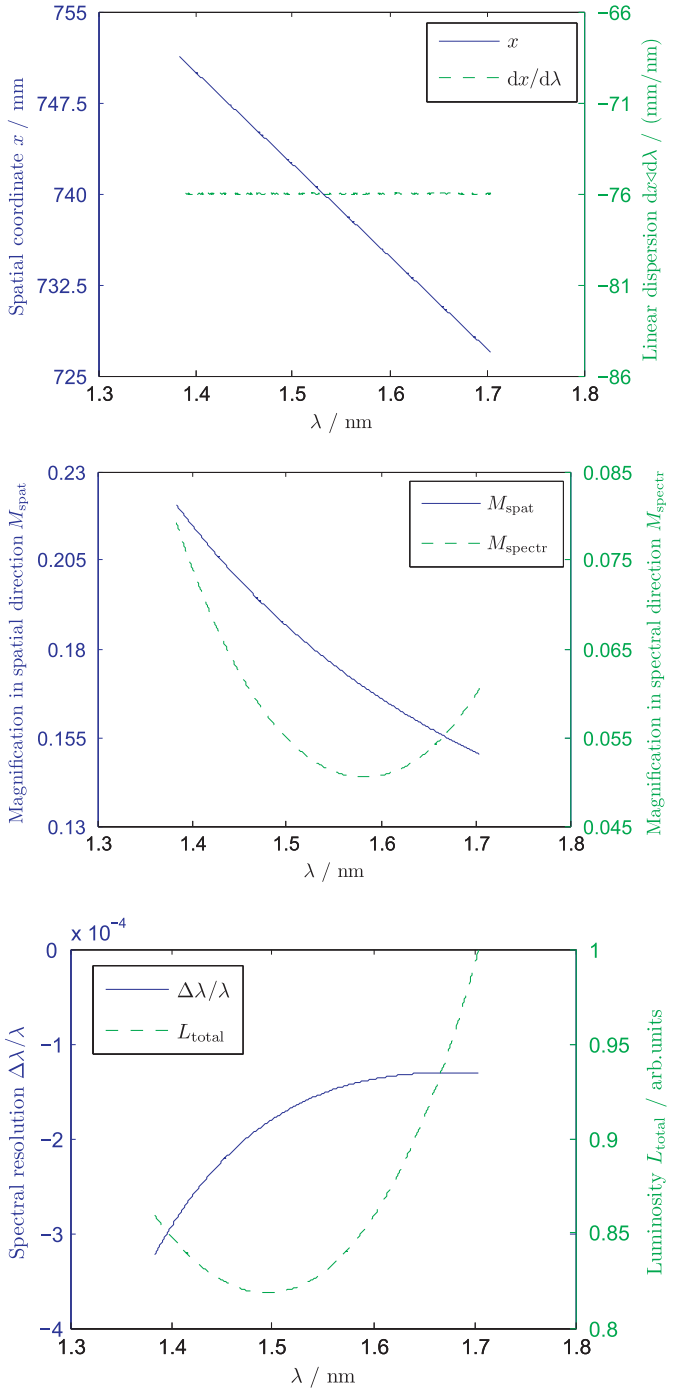

Fig. 11. The major parameters (x, $\mathrm{d}x/\mathrm{d}\lambda$, M_{spat}, M_{spectr}, $\Delta\lambda/\lambda$, $Ł_{\mathrm{total}}$) of a FSSRUD as a function of wavelength λ. The initial conditions r_0 is 775 mm and r_0' is -462 mm, the constant linear dispersion K is set as -76 mm/nm, crystal $2d$ spacing is 1.984 nm and the source size ΔS is 2 mm.

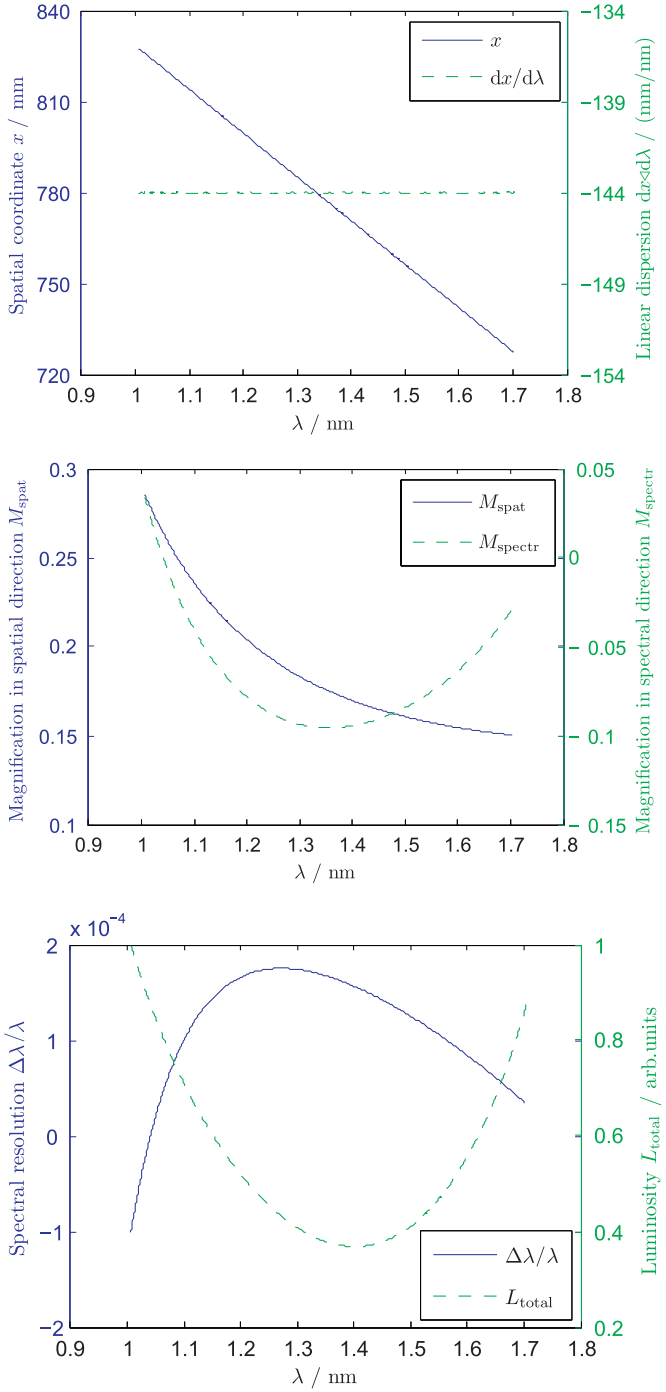

Fig. 12. The major parameters (x, $\mathrm{d}x/\mathrm{d}\lambda$, M_{spat}, M_{spectr}, $\Delta\lambda/\lambda$, $Ł_{\mathrm{total}}$) of a FSSRUD as a function of wavelength λ. The initial conditions r_0 is 775 mm and r_0' is -462 mm, the constant linear dispersion K is set as -144 mm/nm, crystal $2d$ spacing is 1.984 nm and the source size ΔS is 2 mm.

distribution of radiations and a higher energy concentration (i.e., higher luminosity). The FSSRUD with $K=-144$ mm/nm has a little improvement of spectral resolution compared with the FSSRUD with $K=-76$ mm/nm by sacrificing a little of luminosity.

4. Conclusion

The FSSRUD has been proposed to be an option for diagnosing the hot, dense plasmas. The FSSRUD is a special focusing X-ray spectrograph with spatial resolution, which satisfies the condition of uniform dispersion. Comparing with the pure focusing X-ray spectrographs, FSSRUD is convenient in spectrum recording, identification, and can be designed flexibility to satisfy certain experimental requirements. The analysis method developed for the focusing X-ray spectrograph is also helpful for designing the new spectrograph and evaluating its capabilities.

Acknowledgment

This work was supported by the National Natural Science Foundation of China under Grant no. 11005098.

Appendix A. Deducing of the magnification in the meridional plane

If a general coordinate system for the focusing X-ray spectrograph is built as shown in Fig. 13, by using the ray tracing method presented in Section 2.2, the spatial coordinate x for the intersection point of the reflected ray with the X axis can be presented as in the following form:

$$x=\frac{r[s(r^2-r'^2)\sin\varphi-2rr'(s\cos\varphi+r)]}{(r^2-r'^2)(2s\cos\varphi+r)\sin\varphi-2rr'(s\cos2\varphi+r\cos\varphi)}. \tag{A.1}$$

Correspondingly, the wavelength λ is

$$\lambda=\frac{2d}{n}\frac{r^2+s(r\cos\varphi+r'\sin\varphi)}{\sqrt{(r^2+s^2+2rs\cos\varphi)(r^2+r'^2)}}. \tag{A.2}$$

It can be seen that Eqs. (6) and (7) are just the special case of Eqs. (A.1) and (A.2) for $s=0$.

Since the source size is proportional to the image size on the detector plane and affects the spectral resolution, it is important to determine the magnification in the meridional plane which is defined as the ratio of image size Δx to source size $\Delta s\sin\varphi$ along the direction perpendicular to the incident ray direction in the meridional plane

$$M_{\mathrm{spectr}}=\frac{\Delta x}{\Delta s\sin\varphi}=\left(\frac{\partial x}{\partial s}+\frac{\partial x}{\partial\varphi}\frac{\mathrm{d}\varphi}{\mathrm{d}s}\right)\csc\varphi. \tag{A.3}$$

Due to monochromatic imaging, it simultaneously satisfy the condition

$$\frac{\partial\lambda}{\partial s}+\frac{\partial\lambda}{\partial\varphi}\frac{\mathrm{d}\varphi}{\mathrm{d}s}=0. \tag{A.4}$$

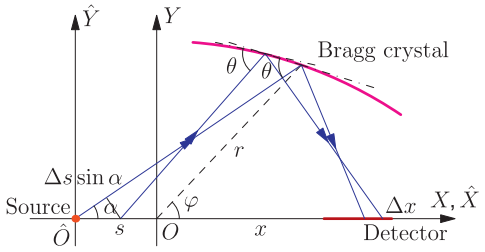

Fig. 13. Coordinate system built for the focusing X-ray spectrograph in which the source is located on X axis but not at origin.

Substituting Eq. (A.4) to Eq. (A.3), it gives

$$M_{\mathbf{spectr}}=\left(\frac{\partial x}{\partial s}-\frac{\partial x}{\partial\varphi}\frac{\partial\lambda}{\partial s}\Big/\frac{\partial\lambda}{\partial\varphi}\right)\csc\varphi. \tag{A.5}$$

Computing the partial derivatives in Eqs. (A.1) and (A.2) and setting $s=0$ in Eq. (A.5) give a simplified expression for the magnification in meridional plane as presented in Eq. (11).

References

[1] S.A. Pikuz, A.I. Erko, A.Ya. Faenov, AIP Conf. Proc. 299 (1993) 544.
[2] I.Yu. Skobelev, et al., JETP 81 (1995) 692.
[3] V. Hamos, Z. Kristallogr. 101 (1939) 17.
[4] F. Bijkerk, E. Louis, G.E. van Dorssen, A.P. Shevelko, A.A. Vasilyev, Appl. Opt. 33 (1994) 82.
[5] J.C. Kieffer, M. Chaker, C.Y. Cote, Y. Beaudoin, H. Ppin, C.Y. Chien, S. Coe, G. Mourou, Appl. Opt. 32 (1993) 4247.
[6] P. Beiersdorfer, M.H. Chen, R.E. Marrs, M.A. Levin, Phys. Rev. A 41 (1990) 3453.
[7] S.A. Pikuz, T.A. Shelkovenko, M.D. Mitchell, K.M. Chandler, J.D. Douglass, R.D. McBride, D.P. Jackson, D.A. Hammer, Rev. Sci. Instrum. 77 (2006) 10F309; S.A. Pikuz, T.A. Shelkovenko, M.D. Mitchell, K.M. Chandler, J.D. Douglass, R.D. McBride, D.P. Jackson, D.A. Hammer, Rev. Sci. Instrum. 41 (1990) 3453.
[8] M. Bitter, B. Fraenkel, K.W. Hill, H. Hsuan, S. von Goeler, Rev. Sci. Instrum. 66 (1995) 530.
[9] B.F.K. Young, A.L. Osterheld, D.F. Price, R. Shepherd, R.E. Stewart, A.Ya. Faenov, A.I. Magunov, T.A. Pikuz, I.Yu. Skobelev, F. Flora, S. Bollanti, P. Di Lazzaro, T. Letardi, A. Grilli, L. Palladino, A. Reale, A. Scafati, L. Reale, Rev. Sci. Instrum. 69 (1998) 4049.
[10] J. Workman, G.A. Kyrala, Rev. Sci. Instrum. 72 (2001) 674.
[11] O.N. Rosmej, J. Wieser, M. Geissel, F. Rosmej, A. Blakevic, J. Jacoby, E. Dewald, M. Roth, E. Brambrinz, K. Weyrich, D.H.H. Hoffmann, T.A. Pikuz, A.Ya. Faenov, A.I. Magunov, I.Yu. Skobelev, N.G. Borisenko, V.P. Shevelko, A.A. Golubev, A. Fertman, V. Turtikov, B.Yu. Sharkov, Nucl. Instr. and Meth. A 495 (2002) 29.
[12] M. Bitter, K.W. Hill, B. Stratton, A.L. Roquemore, D. Mastrovito, S.G. Lee, J.G. Bak, M.K. Moon, U.W. Nam, G. Smith, J.E. Rice, P. Beiersdorfer, B.S. Fraenkel, Rev. Sci. Instrum. 75 (2004) 3660.
[13] S.A. Pikuz, D.B. Sinars, T.A. Shelkovenko, K.M. Chandler, D.A. Hammer, G.V. Ivanenkov, W. Stepniewski, I.Yu. Skobelev, Phys. Rev. Lett. 89 (2002) 035003.
[14] B.M. Song, S.A. Pikuz, T.A. Shelkovenko, K.M. Chandler, M.D. Mitchell, D.A. Hammer, Rev. Sci. Instrum. 69 (2003) 3.
[15] T.A. Shelkovenko, S.A. Pikuz, D.A. Hammer, D.J. Ampleford, S.N. Bland, S.C. Bott, J.P. Chittenden, S.V. Lebedev, Rev. Sci. Instrum. 75 (2004) 3681.
[16] D.B. Sinars, D.F. Wenger, K.L. Keller, G.A. Rochau, J.L. Porter, Rev. Sci. Instrum. 77 (2006) 10F327.
[17] D.F. Wenger, D.B. Sinars, G.A. Rochau, J.E. Bailey, J.L. Porter, A.Ya. Faenov, T.A. Pikuz, S.A. Pikuz, Rev. Sci. Instrum. 77 (2006) 10F312.
[18] T.A. Shelkovenko, D.A. Chalenski, K.M. Chandler, J.D. Douglass, J.B. Greenly, D.A. Hammer, B.R. Kusse, R.D. McBride, S.A. Pikuz, Rev. Sci. Instrum. 77 (2006) 10F521.
[19] S.A. Pikuz, J.D. Douglass, T.A. Shelkovenko, D.B. Sinars, D.A. Hammer, Rev. Sci. Instrum. 79 (2008) 013106.